Arch. Metall. Mater. **67** (2022), 1, 251-254

DOI: https://doi.org/10.24425/amm.2022.137498

P. REZAEI-SHAHREZA[1*], H. REDAEI[1], P. MOOSAVI[1], S. HASANI[1], A. SEIFODDINI[1], B. JEŻ[2], M. NABIAŁEK[2]

EFFECT OF COOLING RATE ON MECHANICAL PROPERTIES OF NEW MULTICOMPONENT Fe-BASED AMORPHOUS ALLOY DURING ANNEALING PROCESS

Fe-based bulk metallic glasses (BMGs) have been extensively investigated due to their ultrahigh strength and elastic moduli as well as desire magnetic properties. However, these BMGs have few applications in industrial productions because of their brittleness at room temperature. This study is focused on the effect of cooling rate on the mechanical properties (especially toughness) in the $Fe_{41}Co_7Cr_{15}Mo_{14}Y_2C_{15}B_6$ BMG. For this aim, two samples with the mentioned composition were fabricated in a water-cooled copper mold with a diameter of 2 mm, and in a graphite mold with a diameter of 3 mm. The formation of crystalline phases of $Fe_{23}(B,C)_6$, α-Fe and Mo_3Co_3C based on XRD patterns was observed after the partial crystallization process. To determine the toughness of the as-cast and annealed samples, the indentation technique was used. These results revealed that the maximum hardness and toughness were depicted in the sample casted in the water-cooled copper mold and annealed up to 928°C. The reason of it can be attributed to the formation of crystalline clusters in the amorphous matrix of the samples casted in the graphite mold, so that this decrease in the cooling rate causes to changing the chemical composition of the amorphous matrix.

Keywords: Bulk metallic glasses (BMGs); Nanocomposite; Mechanical testing; Fracture toughness

1. Introduction

The Fe-based amorphous alloys are used as new materials with a special combination of superior chemical [1-3], magnetic [4,5] and mechanical properties [6-8], which is very important in terms of technology in the last decade. Understanding their mechanical behavior makes them more important for use as advanced engineering materials due to the high strength and low cost of these alloys [9,10]. However, their low ductility has severely limited their application in the industry [11,12]. Therefore, this problem can be overcome by two methods including nano-crystalline phases formation in the amorphous matrix during annealing process [13-15], and minor addition of the alloying elements [16-18]. For instance, Jaafari et al. [15] reported that the ductility of $[(Fe_{0.9}Ni_{0.1})_{77}Mo_5P_9C_{7.5}B_{1.5}]_{99.9}Cu_{0.1}$ amorphous alloy increases due to the reduction of crack length and the increase in shear band density during the crystallization process. Also, the structure and magnetic properties of FeSiBPCu alloys in the presence of appropriate amounts of phosphorus (P) and copper (Cu) was investigated in elsewhere [17]. Based on the results, the nanoparticles of α-Fe clusters with a size of 2-3 nm have been formed and thereby the highest saturation magnetization is obtained [17]. Therefore, the effect of partial crystallization and minor addition of Cu on the magnetic and mechanical properties of $Fe_{41}Co_7Cr_{15}Mo_{14}Y_2C_{15}B_6$ amorphous alloy during crystallization was discussed in detail elsewhere [19,20]. In other words, the results showed that increasing the presence of nanocrystals in the amorphous matrix and partial addition of Cu leads to improved hardness and ductility at various temperature ranges [19,20]. Therefore, in this paper, the effect of cooling rate on mechanical properties of new multicomponent $Fe_{41}Co_7Cr_{15}Mo_{14}Y_2C_{15}B_6$ bulk metallic glasses (BMGs) is investigated before and after the annealing treatment. For this purpose, the studied alloy are cast in the copper and graphite (G) molds with diameters of 2 and 3 mm, respectively, then the specimen are annealed up to temperatures, which were determined based on thermal analysis tests. Finally, the X-ray diffraction (XRD) and hardness test are used to obtain the relationship between phase evolution and its dependent mechanical properties.

[1] YAZD UNIVERSITY, DEPARTMENT OF MINING AND METALLURGICAL ENGINEERING, 89195-741, YAZD, IRAN
[2] CZĘSTOCHOWA UNIVERSITY OF TECHNOLOGY, FACULTY OF PRODUCTION ENGINEERING AND MATERIALS TECHNOLOGY, DEPARTMENT OF PHYSICS, 19 ARMII KRAJOWEJ AV., 42-200 CZĘSTOCHOWA, POLAND

* Corresponding author: parisarezaei88@yahoo.com

2. Materials and methods

The master alloys with nominal composition of $Fe_{41}Co_7Cr_{15}Mo_{14}Y_2C_{15}B_6$ were fabricated in a vacuum arc remelting (VAR) under a Ti-gettered argon atmosphere. Each pre-alloy was remelted several times to emphasize the homogeneity of the composition. Then, amorphous alloys were produced by injection casting in a copper mold with a diameter of 2 mm (C2) and graphite mold with 3 mm (G3) in diameter and 70 mm in length. The thermal stability of the as-cast specimens were obtained by using a differential scanning calorimetry (DSC, NETZSCH DSC 404C) with the heating rates of 5, 10, and 20°C/min. The annealing temperatures of the samples were extracted from the DSC curve (640, 690, 740, and 930 °C for first (I), second (II), third (III), and fourth (IV) exothermic peaks, respectively). Then specimens from the alloys casted in both molds were annealed up to these temperatures with a heating rate of 20°C/min. Phase analysis of the samples was examined by using X-ray diffraction (X'Pert MPD Philips diffractometer) with Cu Kα incident radiation. Moreover, the microhardness of the samples was performed by a Vickers hardness instrument (MH3 KOOPA) with a load of 5 N and a loading time of 10 seconds.

3. Results

Fig. 1 displays the XRD patterns of the as-cast (G3) and annealed specimens in the temperature range of 640, 690, 740, and 930 °C. The formation of crystalline phases of $Fe_{23}(B, C)_6$, α-Fe and Mo_3Co_3C based on XRD patterns is observed in different stages of crystallization process. Also, similar patterns for as-cast (C2) are presented in another paper [24-22].

The average of crystallites size for all specimens is calculated by using the Debye-Scherrer Equation (1) [25]:

$$D = \frac{K\lambda}{\beta \cos\theta} \tag{1}$$

where D, K, λ, θ, and β are the crystallite size; dimensionless shape factor; the wavelength of X-ray, the angle of Bragg, and the half-width of the X-ray diffraction peak, respectively. According to Eq. (1), the average of nanocrystals size for all annealed specimens is listed in Table 1. As presented in Table 1, the average of nanocrystals size increases with a decrease in the cooling rate. For instance, this structural parameter increases from 58 to 73 nm at the fourth crystallization stage in the G3 alloy as compared with the C2 alloy. Also, the volume fraction of crystalline phases (V_f) is obtained by using the XRD patterns (based on the ratio of the integrated areas of the amorphous and the crystalline peaks [26-28]). In other words, it can be measured using the following equation and is listed in Table 2.

$$V_f = \frac{A_{cryst.}}{A_{cryst.} + A_{amor.}} \tag{2}$$

where the integral area of the crystalline and amorphous phases are represented by the $A_{crysr.}$ and $A_{amor.}$ symbols, respectively. According to Table 1, the results show that with an increase in crystallization temperature, volume fraction of the crystalline phases in specimens casted in the both molds is increased. However, in the specimens casted in the C2, it shows that there is more volume fraction of the crystalline phase compared with the specimens casted in the G3. In other words, with a decrease in cooling rate, the size of nanocrystals and their volume fraction during crystallization are decreased.

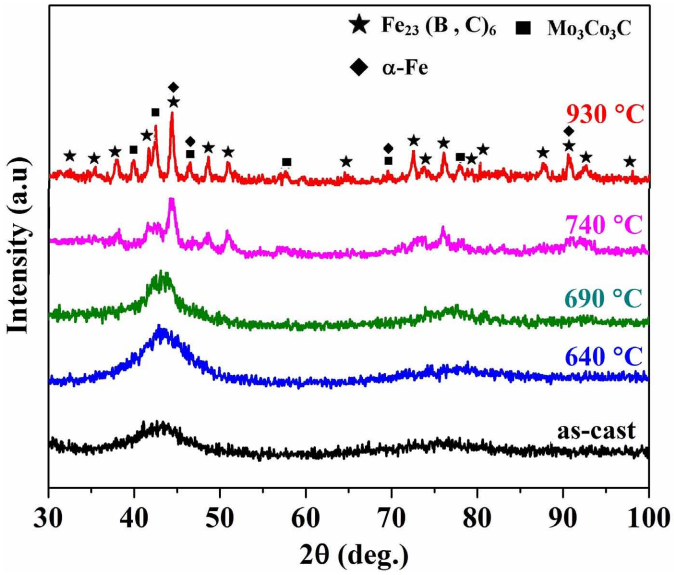

Fig. 1. XRD patterns of the G3 alloy annealed up to different temperatures (640, 690, 740, and 930°C) with a heating rate of 20°C/min

TABLE 1

Volume fractions of crystalline phases and the average of crystallites size in the samples annealed up to temperature ranges of every crystallization peaks

Peak No.	Sample code	Volume Fraction of Crystalline Phases (%)	Average Crystallite Size (nm)	Ref.
			Debye-Scherrer	
I	**G3**	**6.9**	**38**	This work
	C2	7.1	32	[20]
II	G3	12.4	56	This work
	C2	27.1	48	[20]
III	G3	42.8	63	This work
	C2	51.3	51	[20]
IV	G3	59.6	73	This work
	C2	72.8	58	[20]

Microhardness of the all specimens is depicted in Table 2. As shown, the hardness of the G3 after annealing in the fourth peak is increased from 1218.1 to 1517.2 HV compared to the as-cast sample, which can be corresponding to the existence of nanocrystals formed in the amorphous matrix. In addition, the mechanism of deformation in brittle alloys can be investigated using a Vickers hardness tester. In fact, the toughness can be calculated based on the cracks formed around the indent [29,30].

In our previous publication [19], the Palmiqvist model was selected based on the mode of cracks in the C2 alloy. Therefore, the G3 alloy follows the mentioned model. For the Palmiqvist crack model, Eq. (3) can be used to obtained toughness [31].

$$K_c = 0.035 \frac{Hv\sqrt{a}}{\phi}\left(\frac{E\phi}{Hv}\right)^{2/5}\left(\frac{l}{a}\right)^{-1/2} \quad (3)$$

where l is the length from the tip of the indentation to the end of the crack; a is referred to the half the diameter of the indentation; c is the sum of l and a; and ϕ is related to the constraint factor. According to Eq. (3), the toughness of these amorphous alloys at different crystallization stages are measured and the obtained results are given in Table 2. On the other hand, the Vickers indentations on the surface of the samples can be examined using SEM. In addition, the SEM images of Vickers indentations from G3 as-cast and its specimens annealed up to 640, 690, 740, and 930°C are represented in Fig. 2. According to the obtained results, the simultaneous increase of toughness and hardness can be related to the increase of volume fraction of the crystallized phases during the partial crystallization process [32,33]. In addition, these results show that the minimum hardness and toughness are observed for the G3 sample annealed up to 930°C. The reason of it can be attributed to the formation of clusters in

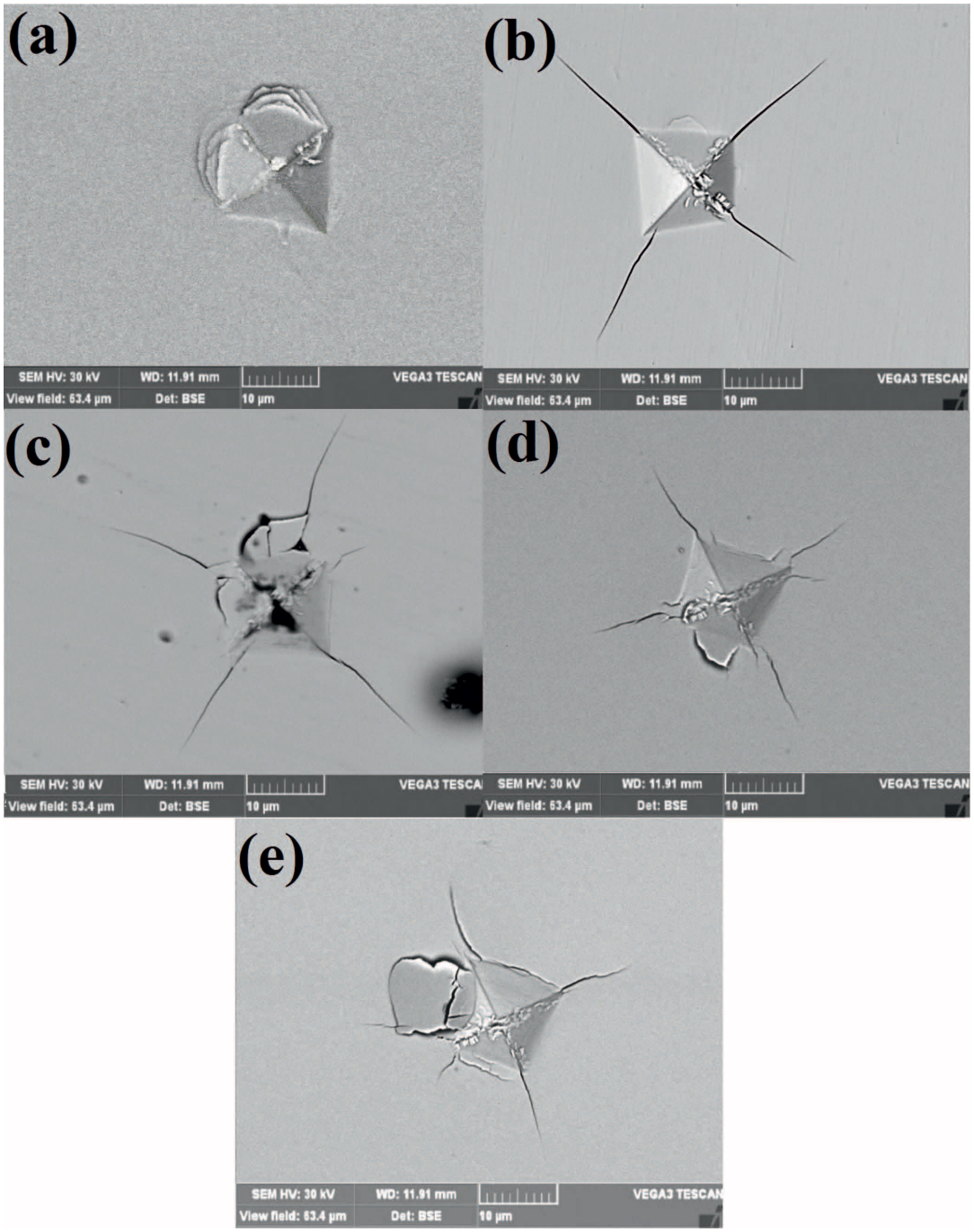

Fig. 2. SEM images of Vickers microhardness for (a) as-cast G3 and its specimens annealed up to (b) 640, (c) 690, (d) 740, and (e) 930°C with a heating rate of 20°C/min

the amorphous matrix of the samples casted in the graphite mold, so that this decrease in the cooling rate causes to changing the chemical composition of the amorphous matrix. For therefore, it is notable that in our previous publication [21], it was shown that the cast alloy with the mentioned composition casted in the graphite mold has higher thermal stability compared to that of the casted in a copper mold.

TABLE 2

Vickers microhardness (HV) and fracture toughness (Kc) corresponding to the as-cast alloys and their specimens annealed up to temperature ranges of every crystallization peaks

Peak No.	Sample code	HV	Kc (MPa√m)	Ref.
As-cast	G3	1218.1	—	This work
	C2	1368.4	—	[20]
I	G3	1328.4	1.9	This work
	C2	1421.9	2.1	[20]
II	G3	1382.6	2.3	This work
	C2	1522.3	3.0	[20]
III	G3	1443.5	2.4	This work
	C2	1662.1	3.5	[20]
IV	G3	1517.2	2.7	This work
	C2	1761.2	4.6	[20]

4. Conclusions

In this work, the effect of cooling rate on mechanical properties of Fe-based bulk metallic glasses (BMGs) before and after annealing treatment was investigated. It was found that the crystalline phases of $Fe_{23}(B, C)_6$, α-Fe, and Mo_3Co_3C based on XRD patterns were formed during four stages of the crystallization process. Also, the results of indentation technique revealed that the maximum hardness and toughness were obtained in the sample casted in the water-cooled copper mold and followed by annealing up to 928 °C. The reason of it can be attributed to the formation of clusters in the amorphous matrix of the samples casted in the graphite mold, so that this decrease in the cooling rate causes to changing the chemical composition of the amorphous matrix and thermal stability of this sample.

REFERENCES

[1] H. Jiang, T. Shang, H. Xian, B. Sun, Q. Zhang, Q. Yu et al., Small Struct. **2000057** (2020).

[2] W. Yang, Q. Wang, W. Li, L. Xue, H. Liu, J. Zhou et al., Mater. Des. **161**, 136-46 (2019).

[3] L. Liu, C. Zhang, Thin Solid Films **561**, 70-86 (2014).

[4] P. Pietrusiewicz, M. Nabiałek, B. Jeż, Materials (Basel) **13**, 4962 (2020).

[5] M. Nabiałek, B. Jeż, K. Błoch, J. Gondro, K. Jeż, A.V. Sandu, P. Pietrusiewicz, J. Alloys Compd. **820**, 153420 (2020)

[6] W. Guo Y. Wu, J. Zhang, S. Hong, G. Li, G. Ying et al., J. Therm. Spray Technol. **23**, 1157-80 (2014).

[7] B.S. Oliveira, D.H. Milanez, D.R. Leiva, L.I.L. Faria, W.J. Botta, C.S. Kiminami, Mater. Res. **20**, 89-95 (2017).

[8] Y. Han, F.L. Kong, F.F. Han, A. Inoue, S.L. Zhu, E. Shalaan et al. Intermetallics **76**, 18-25 (2016).

[9] A. Hitit, H. Şahin, Metals (Basel) **7**, 7 (2016).

[10] P.H. Tsai, C.I. Lee, S.M. Song, Y.C. Liao, T.H. Li, J.C. Jang et al., Coatings **10**, 1212 (2020).

[11] V. Keryvin, V.H. Hoang, J. Shen, Intermetallics **17**, 211-7 (2009).

[12] J. Zhou, Q. Wang, X. Hui, Q. Zeng, Y. Xiong, K. Yin et al., Mater. Des. **191**, 108597 (2020).

[13] A. Masood, V. Ström, L. Belova, K.V. Rao, J.J. Ågren, Appl. Phys. **113**, 013505 (2013).

[14] S. Zhang, D. Sun, Y. Fu, H. Du, Surf. Coatings Technol. **167**, 113-9 (2003).

[15] Z. Jaafari, A. Seifoddini, S. Hasani, Metall. Mater. Trans. A **50**, 2875-85 (2019).

[16] Z. Dan, Y. Yamada, Y. Zhang, M. Nishijima, N. Hara, H. Matsumoto et al., Mater. Trans. **54**, 561-5 (2013).

[17] A. Makino, H. Men, T. Kubota, K. Yubuta, A. Inoue, J. Appl. Phys. **105**, 07A308 (2009).

[18] S. Wang, W. Jiang, H. Hu, P. Liu, J. Wu, B. Zhang, Prog. Nat. Sci. Mater. Int. **27**, 503-6 (2017).

[19] P. Rezaei-Shahreza, A. Seifoddini, S. Hasani, J. Alloys Compd. **738**, 197-205 (2018).

[20] S. Hasani, P. Rezaei-Shahreza, A. Seifoddini, Metall. Mater. Trans. A **50**, 63-71 (2019).

[21] H. Redaei, P. Rezaei-Shahreza, A. Seifoddini, S. Hasani, Acta Phys. Pol. A **138**, 265-7 (2020).

[22] P. Rezaei-Shahreza, A. Seifoddini, S. Hasani, J. Non-Crystalline Solids **471**, 286-294 (2017).

[23] P. Rezaei-Shahreza, A. Seifoddini, S. Hasani, Thermochimica Acta **652**, 119-125 (2017).

[24] S. Hasani, P. Rezaei-Shahreza, A. Seifoddini, Thermal Analysis and Calorimetry **143**, 3365-3375 (2021).

[25] P. Scherrer, Bestimmung der inneren Struktur und der Größe von Kolloidteilchen mittels Röntgenstrahlen. Kolloidchem. Ein Lehrb., Berlin, Heidelberg: Springer Berlin Heidelberg, 387-409 (1912).

[26] T. Gloriant, M. Gich, S. Suriñach, M.D. Baró, A.L. Greer, J. Metastable Nanocrystalline Mater. **8**, 365-70 (2000).

[27] S. Cardinal, J.M. Pelletier, M. Eisenbart, U.E. Klotz, Mater. Sci. Eng. A **660**, 158-65 (2016).

[28] S. Enzo, S. Polizzi, A. Benedetti, Zeitschrift Für Krist **170**, 275-87 (1985).

[29] V. Keryvin, X.D. Vu, V.H. Hoang, J. Shen, J. Alloys Compd. **504**, S41-4 (2010).

[30] H.W. Zhang, G. Subhash, X.N. Jing, L.J. Kecskes, R.J. Dowding, Philos. Mag. Lett. **86**, 333-45 (2006).

[31] G.R. Antist, P. Chantikul, B.R. Lawn, D.B. Marshall, J. Am. Ceram. Soc. **64**, 533-8 (1981).

[32] Y. He, G.J. Shiflet, S.J. Poon, Acta Metall. Mater. **43**, 83-91 (1995).

[33] C. Suryanarayana, Mater. Today **15**, 486-98 (2012).